Compact Range Quiet Zone Modelling:

Quantitative Assessment using a Variety of Electromagnetic Simulation Methods

C.G. Parini, R. Dubrovka
Queen Mary University of London
School of Electronic Engineering and Computer Sciences
Peter Landin Building, London, UK
c.g.parini@qmul.ac.uk, r.dubrovka@qmul.ac.uk

S.F. Gregson
Nearfield Systems Inc.
19730 Magellan Drive
Torrance, California, USA
sgregson@nearfield.com

***Abstract*—This paper presents the results of a recent computational electromagnetic (CEM) simulation campaign for a single offset reflector CATR, where a number of models employing different field propagation methods were compared and contrasted both qualitatively and quantitatively using objective, non-local statistical image classification techniques.**

Keywords—compact antenna test range, computational electromagnetic, quiet-zone, simulation, geometrical optics, physical optics, current-elements, FEKO.

I. Introduction

The single-offset compact antenna test range (CATR) is a widely deployed technique for broadband characterization of electrically large antennas at reduced range lengths [1, 2]. The nature of the curvature and location of the offset parabolic reflector as well as the edge geometry ensures that the resulting collimated field is comprised locally of a pseudo plane-wave. The coupling of this plane-wave into the aperture of the test antenna creates the classical measured "far-field" radiation pattern. The accuracy of a pattern measured using a compact range is primarily determined by the uniformity of the phase and amplitude of the pseudo plane-wave illuminating the AUT aperture. The quality of the pseudo plane-wave is governed primarily by two factors: amplitude and phase taper (which is imposed by the radiation pattern of the feed and its location with respect to the reflector focus), and reflector edge diffraction (which usually manifests as a high spatial frequency ripple in the pseudo plane wave) [2]. Thus, CATR performance is generally specified in terms of the amplitude and phase ripple throughout a finite region of space, called the quiet-zone (QZ). As the configuration of the reflector edge treatment is so inextricably linked to the purity of the pseudo-plane wave, many different modelling techniques have been employed over the years to produce accurate simulations that can be used to optimize the design of the CATR.

In general, it is difficult to obtain closed form functional solutions for the electromagnetic (EM) field at an arbitrary point in space from knowledge of the tangential electric and/or tangential magnetic fields over a closed surface for anything but the simplest of configurations. As such, recourse to alternative, typically numerical based techniques becomes unavoidable. In essence, any antenna measurement can be simulated by evaluating the complex coupling coefficient between the feed and the field probe. This must be accomplished for each point within the simulated CATR quiet zone acquisition surface, for each sampled polarization, and for each frequency at which the measurement is to be taken. In principle then, it would be possible to obtain the mutual coupling coefficient, S21, between a given mode in the waveguide port in the feed and a given mode in the waveguide port of the test antenna from a three-dimensional computational electromagnetic (CEM) full wave solver. This approach would have the advantage of, potentially, introducing the least number of assumptions and approximations and therefore could in principle yield the most accurate predictions. Unfortunately, at the present time, although many solvers are available these are generally considered inappropriate for simulating problem spaces as electrically large as those needed to enclose a complete CATR system, as illustrated in Figure 1, particularly at higher frequencies, *e.g.* short cm-wave, mm-wave frequencies and above and especially when that simulation is to be incorporated within a design optimisation. This limitation is merely a consequence of the extended processing times and the large amounts of computer resources that are typically required. Hence, alternative, perhaps less generally applicable, but more computationally efficient techniques are required. However, the significance that the reflector edge treatment has on the quality of the pseudo plane wave in the CATR QZ, as expounded above, means that special emphasis must be placed upon the successful validation and verification of any performance prediction software that is harnessed in the design of a CATR. The following section provides an introduction to the CEM CATR model before giving an overview to the five simulation methods what were employed.

II. Overview of CEM Model

A schematic representation of the geometry of a CATR configuration can be seen presented in Figure 1 below. Here, the parabolic reflector had a 3.6576 m (12 foot) focal length. The surface profile of the CATR was assumed to be formed from a concave paraboloidal surface. The reflector surface must be a paraboloid of revolution so that the, assumed spherical, incident wave propagating from the focus of the reflector is collimated into a pseudo plane-wave. The CATR reflector included serrations formed from triangular petals. The phase centre of the feed was placed at the focus of the offset reflector and the feed was tilted up in elevation by 28°. A WR430 circular choked waveguide was used for the feed with far-field data being provided by a proprietary full-wave three-dimensional CEM solver using the finite difference time-domain technique. The origin of the CATR co-ordinate system was located at the vertex of the parabolic reflector with the QZ simulations being computed over a transverse plane at $z = 1.8f$ where f was the focal length of the reflector. This is a non-

optimal CATR design but serves as a suitable comparison vehicle for this study.

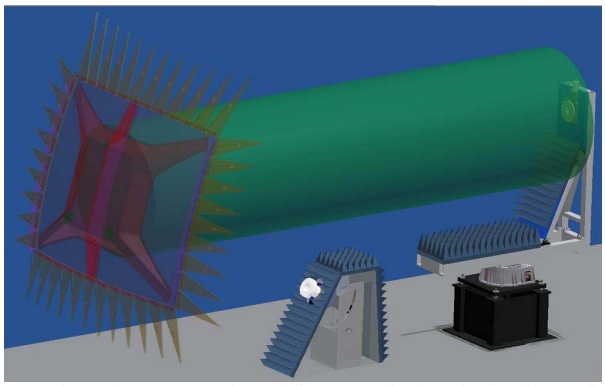

Fig. 1. Schematic representation of the serrated edge single offset-reflector CATR being simulated. The greed cylinder represents the direction of propagation of the pseudo-plane wave.

The field illuminating the reflector is determined from far-field antenna pattern function by reintroducing the spherical phase function and the inverse r term. The corresponding magnetic field (as required by some of the field propagation models described below) was calculated from the electric field assuming the TEM far-field condition. Thus, each of the CATR simulations assumes that the reflector is in the far-field of the feed which was a condition easily satisfied by the electrically small feed antenna. This pattern could be derived from computational electromagnetic simulation, or from empirical range measurement. When introducing the feed into the CATR model it is assumed that the phase centre of the feed is coincident and synonymous with the focus of the CATR paraboloidal reflector. Also, as a result of the requirement to minimize feed induced blockage, an offset reflector design is harnessed. Here, it is assumed that the vertex of the reflector is coincident with the bottom edge of the reflector. Thus, the feed is required to be tilted up in elevation so that the boresight direction is orientated towards the centre of the reflector surface. A vector isometric rotation was used to implement this pattern rotation [2, 3]. In practice as a result of the spherical loss, the feed is usually tilted up a little beyond the geometrical centre of the reflector so as to equalize the reflector illumination. In these simulations this was not done and the resulting QZ predictions are sub-optimum. This compromise was admitted on the basis it enabled a wider range of simulations to be directly compared.

A crucial feature of the CATR quiet-zone performance prediction is the effect that the truncation of the offset-reflector will have on the collimated fields and the resulting edge diffraction effects. In practice, this is incorporated into the model by reducing the limits of integration to only include the region bound by an arbitrarily shaped closed polygon that lies within the xy-axis. Such an approach is accurate providing the reflector is more than a few wavelengths across. This is the basis of the physical optics approximation and it is used extensively when treating electromagnetic scatting problems [4]. Thus, the surface current will only be assigned a value over the illuminated region of the reflector surface. Therefore in the shadow region that is cast by the surface the currents are assumed to be identically zero. Hence we can expect that this method will be unsuitable for predicting the fields in the deep shadow region where these neglected currents can be reasonably expected to constitute the majority current sources. However, this region is outside of the area of interest when modelling the quiet-zone performance of a CATR.

III. Introduction to Modelling Methods

This section presents an overview of the five CEM modelling techniques that were used to produce the various CATR QZ predictions presented below in Section IV.

A. *Geometrical Optics with Geometrical Theory of Diffraction Method*

Geometrical optics (GO), or ray optics takes the Lagrangian point of view by considering the transportation of energy quanta from a point of emission to a point of absorption and is applicable to problems where the frequency is sufficiently high to enable the wave properties of light to be ignored giving rise to an infinite frequency approximation [4]. Thus, GO is an incomplete treatment of the physical phenomena and needs to be augmented to include diffraction effects which are so crucial when predicting the QZ of a CATR. In practice this can be implemented by incorporating a geometrical theory of diffraction (GTD) correction [4] through the principle of linear superposition with a detailed treatment of GO & GTD being presented within that reference.

B. *Vector Huygens Method (PWS Method)*

The field reflected by the CATR reflector can be computed from the General Law of Reflection. This states that if a homogeneous plane wave is incident on a perfect electrical conducting (PEC) flat surface of infinite extent, the normal component of the reflected field is unchanged upon reflection whilst the tangential components of the electric field are reversed in sign. This can be taken to represent the general form of the law of reflection with the scattered field being a plane wave as the material is assumed to be infinite in extent in the tangential direction and the material properties do not vary across this surface.

Once the field reflected by the main reflector is known across the surface of the reflector, the Vector-Huygens method can be used to compute the field across the quiet-zone [3]. The vector-Huygens method is a powerful technique for determining the field in a source and sink free region outside a surface from knowledge of the field distribution over that surface. It is applicable to arbitrary but smoothly shaped (not necessarily planar) apertures over which the tangential components of the electric fields are prescribed. The vector Huygens principle can be obtained directly from the co-ordinate free form of the plane-wave spectrum method (PWS) plane-rectilinear near-field to far-field transformation by collapsing the area of the aperture plane until in the limit it becomes a single elemental, *i.e.* infinitesimal, Huygens source [3]. When expressed mathematically, providing the scalar product of the surface unit normal and the vector to the field point are positive, the electric field at a point P radiated by a closed Huygens surface S that is in the far-field of the infinitesimal Huygens element is given by [3],

$$d\underline{E}_p(P) = \frac{jda}{\lambda}\hat{\underline{u}}_r \times (\underline{E} \times \hat{\underline{n}})\psi \quad (1)$$

Here, ψ is the free space Green's function, $\underline{E}$ is the reflected electric field, $\underline{n}$ is the unit surface normal and $\underline{u}_r$ is the direction to the field point P located at (x, y, z), must be in the far-field of the infinitesimal radiating elemental Huygens source, which results in the field point being removed from the Huygens source by a few wavelengths. Thus, the total field at a point in space can be expressed by integrating across the complete radiating surface. Hence, for the purposes of simulating a CATR, providing the QZ is more than a couple of wavelengths from the reflector (which it always will be) the results will be valid. Here, the unit surface normal can be obtained from [3],

$$\hat{\underline{n}} = \nabla\phi / \|\nabla\phi\| \quad (2)$$

Where, the surface profile is expressed as,

$$\phi(x, y, z) = z - f(x, y) \quad (3)$$

C. Kirchoff Huygens Method

The Kirchhoff-Huygens method is a general technique for determining the field in a source and sink free region outside a surface from knowledge of the field distribution over that closed surface [3]. It is applicable to arbitrary but not necessarily smoothly shaped apertures over which the tangential components of the electric *and* magnetic fields are prescribed. The Kirchhoff-Huygens method is in essence a direct integral of Maxwell's equations. The general vector Kirchhoff-Huygens formula can be expressed as [3],

$$d\underline{E}_p = \frac{da}{4\pi}\left[-j\omega\mu(\hat{\underline{n}} \times \underline{H})\psi + (\hat{\underline{n}} \times \underline{E}) \times \nabla\psi + (\hat{\underline{n}} \cdot \underline{E})\nabla\psi\right] \quad (4)$$

In addition to the reflected electric fields $\underline{E}$, this expression requires knowledge of the tangential components of the reflected magnetic fields $\underline{H}$. These can be computed from the incident magnetic fields using the method of images (and again assuming the parabolic reflector is locally planar) [5],

$$\underline{n} \times \underline{H}_i = \underline{n} \times \underline{H}_r \quad (5)$$

Here the subscripts i and r are taken to denote incident and reflected fields respectively. The Kirchhoff Huygens theory is exact, provided that the field is known exactly over a closed surface although this additional rigor is sought as the expense of significant additional computational effort. The closed surface can take the form of an infinite plane together with an infinite radius hemisphere. If the source is finite then, from the radiation condition, it can be seen that no contribution to the total field arises from any part of the hemispherical portion of the surface.

D. Current Elements Method

The current elements method is an alternative field propagation method to those developed above. The current element method replaces the fields with an equivalent surface current density $\underline{J}_s$ which is used as an equivalent source to the original fields. The surface current density across the surface of the reflector can be obtained from the incident magnetic fields and the surface unit normal using [5],

$$\underline{J}_s = 2\hat{\underline{n}} \times \underline{H}_i = 2\hat{\underline{n}} \times \underline{H}_r \quad (6)$$

The surface current density approximation for $\underline{J}_s$ (as embodied by the above expression) is known as the *physical-optics* approximation [5]. The fields radiated by an electric current element can be obtained from the vector potential and the free-space Green's function yielding [6],

$$d\underline{H}(P) = \frac{da}{4\pi}\underline{J}_s \times \nabla\psi \quad (7)$$

This is an exact equation. The corresponding elemental electric fields can be obtained, to a very good approximation, from the elemental magnetic fields using the far-field TEM condition. Again, the field point only need be in the far-field of the elemental source which is a requirement that is satisfied when the separation is larger than a few wavelengths. Integrating the elemental electric and magnetic fields results in the computation of the complete electromagnetic six-vector. In practice, for the case of a CATR with a QZ located at a distance z that is larger than the focal length of the reflector, the difference between the electric field as computed using the TEM condition and the exact formula [6] is typically on the order of the limit of double precision arithmetic.

E. FEKO Physical Optics Method

The proprietary computational electromagnetic simulation tool FEKO [7] was also used to predict CATR QZ. FEKO hybridises the current-based accurate Method of Moments (MoM) with PO whilst a bidirectional coupling between the MoM and PO being maintained in the solution. FEKO triangulates a PO region, exactly the same as it would for a MoM solution. FEKO implements a number of extensions to the PO:

- Fock currents to account for the effect of creeping waves over the shadow boundary region into "unlit" areas.
- Correction terms to achieve more accurate current representation close to edges and wedges.
- Multilevel Fast Multipole Method (MLFMM) hybridisation: the MoM region of a hybrid MoM/PO or MoM/LE-PO problem may be solved with the MLFMM.

Hence, FEKO hybridisation would be ideal for solving large reflector antenna problems taking into account a real feed system or its radiation pattern/near-field distribution where both can be easily introduced as power sources. In general, the FEKO PO solution, as based on surface current distribution, is expected to be the closest to the previously described current element method.

IV. CATR CEM Simulation Results

The five different CEM modelling techniques described above were used to compute QZ performance predictions for the CATR configuration detailed above. The five simulations all used the same feed pattern and geometry with only the field propagation method and reflection calculation changing between the simulations. The simulations were: Geometrical Optics with Geometrical Theory of Diffraction edge correction (GO+GTD), Vector Huygens (VH), Kirchhoff Huygens (KH), Current Elements (CE) and FEKO Physical Optics (FEKO).

Figure 2 below presents a comparison of the CATR QZ amplitude predictions for the five simulations for the horizontally polarised electric field component (E_x) in terms of iso-levels (contours) where each of the patterns were normalised to 0 dB at the peak of the pattern. Here, red contours denote GO+UTD, magenta contours denote VH, cyan contours denote KH blue contours denote CE based field propagation whilst black contours represent the results from FEKO using PO. Figure 3 contains an equivalent plot for the vertically polarised (cross-polar) electric field component, (E_y).

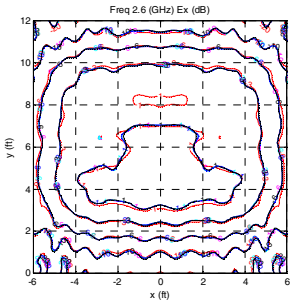

Fig. 2. Comparison of E_x polarised QZ amplitude patterns.

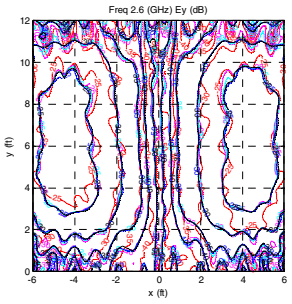

Fig. 3. Comparison of E_y polarised QZ amplitude patterns.

From inspection of these plots it is clear that the VH, KH and CE based methods are in very good agreement with GO+GTD being in only slightly less close agreement with the main difference being the presence of additional ripple on the GO+GTD QZ predictions. General levels and shape of the patterns, for both *x*- and *y*-polarised field amplitude plots are very encouraging. Some asymmetry is apparent in the GO+GTD simulations on the *y*-polarised patterns, which is erroneous as the model is symmetrical in the *yz*-plane. The feed model is not quite perfectly symmetrical which was merely a consequence of small numerical imperfections within the CEM model that was used to generate the feed pattern predictions. The following plots contain horizontal and vertical amplitude and phase plots through the QZ that are intended to enable a more critical assessment of the degree of agreement to be attained.

Here, it is clear that all of the principal polarised cardinal cuts are in good agreement with the general pattern shapes and features being in close agreement. Although not shown due to lack of space, better agreement was attained at higher frequencies where the GO assumption becomes an increasingly good approximation of the physics. General cross-polar levels were also in excellent agreement, with only the null-depth changing between the simulations. As can be seen the CE and FEKO PO models were closest in agreement, especially in the very demanding vertical cross-polar cut (where the levels are *circa* 70 dB below the peak). The phase patterns are also in very good agreement confirming adoption of the same (suppressed) time dependency. Some small phase differences are evident becoming progressively more noticeable in regions of low field intensity where it is difficult to control phase, *e.g.* in nulls and towards the extremities of the QZ. From inspection of the cross-polar iso-level plots and the cardinal cuts, some differences in symmetry (left to right) are evident in the GO+GTD predictions (these are most noticeable in the cross-polar patterns). As both the feed and reflector are symmetrical in this axis, as the offset is in the vertical axis, symmetry should not be broken here and this is an indication of an error within the model. The VH, KH, CE & FRKO PO models *all* exhibit a very good degree of symmetry in this axis.

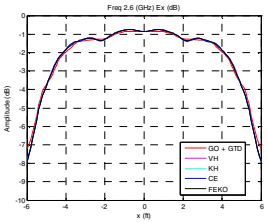

Fig. 4. Horizontal cut through QZ of amplitude of H-pol fields.

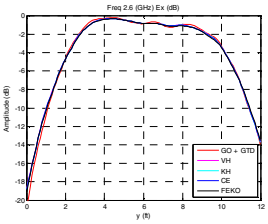

Fig. 5. Vertical cut through QZ of amplitude of H-pol fields.

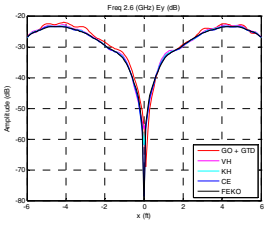

Fig. 6. Horizontal cut through QZ of amplitude of V-pol fields.

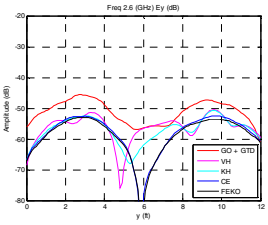

Fig. 7. Vertical cut through QZ of amplitude of V-pol fields.

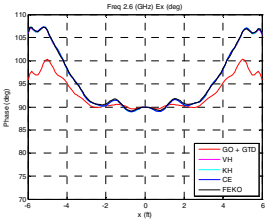

Fig. 8. Horizontal cut through QZ of phase of H-pol fields.

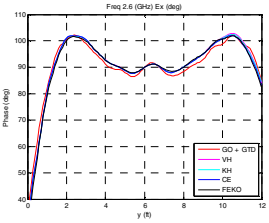

Fig. 9. Vertical cut through QZ of phase of H-pol fields.

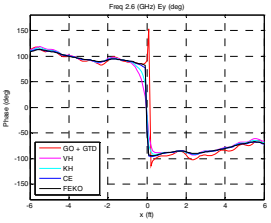

Fig. 10. Horizontal cut through QZ of phase of V-pol fields.

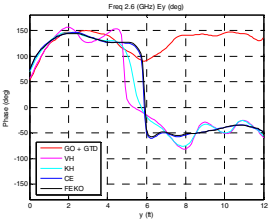

Fig. 11. Vertical cut through QZ of phase of V-pol fields.

V. Statistical Image Classification of Results

As was illustrated within the preceding section, qualitatively, each of the five different CATR QZ simulations were found to be in very good agreement with one another. Furthermore from inspection of the CE & FEKO PO models it could be seen that these arguably demonstrated the closest agreement with the GO+GTD result exhibiting the largest differences. These observations however are merely qualitative and it is preferable to instead adopt quantitative holistic pattern comparison techniques [3, 8]. Many attempts to produce objective quantitative measures of correspondence between data sets that can be used to assess the accuracy, sensitivity and repeatability associated with the production of that data have been have been reported in the open literature [3, 8, 9]. In these, a variety of statistical methods have proved successful in the robust assessment of similarity between antenna pattern functions where the comparison has been found to be complicated: the large amount of interferometric, *i.e.*

complex, data which is used to represent the QZ performance and the huge dynamic range of that data, which in this case is greater than 70 dB. This however, is the first time that these sophisticated techniques have been harnessed to assess near-field data. Two commonly used techniques for the comparison of electromagnetic data are the root mean square (RMS) difference [2] and the ordinal measure of correspondence [3, 8]. Table I contains a comparison of the RMS difference (in dB) which is a conventional interval assessment technique. The larger the negative value of the RMS value the better the agreement with -300 dB corresponding to perfect agreement between the data sets. Conversely, Table II contains an equivalent set of comparisons using the ordinal measure of correspondence k, where zero represents no similarity and unity represents perfect agreement such that $0 \le k \le 1$ [3].

TABLE I. MEAN RMS DIFFERENCE, QZ PATTERNS

	GO	**VH**	**KH**	**CE**	**FEKO**
GO	-300.00	-39.39	-39.20	-38.90	-38.95
VH	-39.39	-300.00	-56.41	-53.50	-49.13
KH	-39.20	-56.41	-300.00	-55.65	-52.38
CE	-38.90	-53.50	-55.65	-300.00	-50.82
FEKO	-38.95	-49.13	-52.38	-50.82	-300.00

TABLE II. ORDINAL MEASURE OF CORRESPONDENCE, QZ PATTERNS

	GO	**VH**	**KH**	**CE**	**FEKO**
GO	1.000	0.734	0.721	0.706	0.708
VH	0.734	1.000	0.965	0.934	0.931
KH	0.721	0.965	1.000	0.962	0.959
CE	0.706	0.934	0.962	1.000	0.972
FEKO	0.708	0.931	0.959	0.972	1.000

Each of these comparison techniques are commutative and as a consequence of this the tables exhibit symmetry as their elements are equal to their transpose elements, *i.e.* $A_{j,k} = A_{k,j}$. The values of the elements in the leading diagonal merely represent perfect agreement between the patterns being compared and have no significance further than that. Thus, in each case the comparison of five simulations (yielding complex dual polarised) data arrays with 121 by 121 elements has been successfully reduced to the assessment of ten quantitative numbers (*i.e.* the elements of the upper triangular matrix shown in dark typeface in Tables I and II). However, while Table I was derived from comparing the amplitudes of the E_x and E_y polarised QZ data, Table II was produced from comparing the amplitude *and* phase patterns of *both* the E_x and E_y polarised QZ fields thereby comprising a far more holistic comparison of much larger data sets.

From inspection of the first row of Tables I and II it is clear that the GO+GTD method is in less encouraging agreement than the other methods in this study, and is essentially an outlier. This is expected and ties in with the results of the visual inspection. From the results shown in Table II it is clear that CE and FEKO PO are in very good agreement with a k value of 0.972. This agrees with inspection of the plots, especially Figures 7, 10 and 11. The KH and VH methods are similar and this too is revealed within the ordinal assessment as shown in Table II. The results of the interval assessment is less clearly defined and stems from the large dynamic range and the very localised region and low level (*i.e.* in vicinity of the cross-polar null) where the largest differences are manifest.

At route, almost all data assessment techniques depend on reducing the dimensionally of the data being assessed to make them more easily accessible. Electromagnetic data may contain tens or hundreds of thousands of individual complex vector data points and the quantitative assessment of such large data sets become close to impossible without distilling the data down to more manageable levels. Clearly, such data reduction techniques almost always involve the loss of some information. However, it should be borne in mind that all inferential statistical methods, be they nominal (*i.e.* categorical), ordinal, interval or ratio abstract the data to assess specific attributes or features so in all forms of statistical data assessment information is lost about the specific nature of the sets being examined. Thus, the choice of assessment technique or must be steered by an informed understanding of the nature of the parameters that are to be assessed.

VI. CONCLUSIONS

A detailed GO, VH, KH, CE, FECO simulation for the QZ field for a single offset reflector CATR has been presented. It was found that for this low frequency case (that is low with respect to the electrical size of the reflector) the CE and FEKO PO simulations were qualitatively and quantitatively in the closest agreement. With the exception of the low amplitude pattern null region, the computationally efficient VH method was found to be in close agreement with the more intensive KH and CE methods. In this paper, for the first time, statistical image classification techniques were successfully used to assess the CATR QZ performance data opening the way for their use as a convergence criteria for a genetic optimiser for the purpose of automated optimisation of CATR designs. The research reported in this paper is on-going with further work investigating the efficient optimisation of CATR configurations underway.

REFERENCES

[1] R.C. Johnson, H.A. Ecker, R.A. Moore, "Compact Range Techniques and Measurements", IEEE Transactions on Antennas and Propagation, September 1969; 11L:568-76.

[2] C.G. Parini, S.F. Gregson, J. McCormick, D. Janse van Rensburg "Theory and Practice of Modern Antenna Range Measurements", IET Press, 2014, ISBN 978-1-84919-560-7.

[3] S.F. Gregson, J. McCormick, C.G. Parini, "Principles of Planar Near-Field Antenna Measurements", IET Press, 2007, ISBN 978-0-86341-736-8.

[4] G.L. James, "Geometrical Theory of Diffraction for Electromagnetic Waves", 3rd Edition, IET Press, 2007, ISBN 978-0-86341-062-8.

[5] W.L. Stutzman, G.A. Theil, "Antenna Theory and Design", 2nd Edition, John Wiley & Sons, Inc., 1998, ISBN 0-471-02590-9.

[6] C.A. Balanis, "Advanced Engineering Electromagnetics", John Wiley & Sons, Inc. 1989, ISBN 0-471-62194-3.

[7] EM Software & Systems, FEKO Suit 7.0, www.feko.info.

[8] S.F. Gregson, A.C. Newell, C. Feat, F. Viguier Vigi, "The Use of Statistical Image Classification In Assessing Antenna Pattern Measurements", AMTA, Columbus Ohio, 2013.

[9] J. McCormick, S.F. Gregson, C.G. Parini, "Quantitative Measure of Comparison between Antenna Pattern Data Sets", IEE Proc.-Microw. Antennas Propag, Vol. 152, No 6, December 2005.